

Manuscript Number: EPSL-D-15-00732R2

Title: Constraining multi-stage exposure-burial scenarios for boulders preserved beneath cold-based glacial ice in Thule, Northwest Greenland

Article Type: Letters

Keywords: geochronology; cosmogenic nuclides; Polar Regions; cold-based ice; till recycling; Quaternary

Corresponding Author: Ms. Lee B Corbett,

Corresponding Author's Institution: University of Vermont

First Author: Lee B Corbett

Order of Authors: Lee B Corbett; Paul R Bierman; Dylan H Rood

Abstract: Boulders and landscapes preserved beneath cold-based, non-erosive glacial ice violate assumptions associated with simple cosmogenic exposure dating. In such a setting, simple single isotope exposure ages over estimate the latest period of surface exposure; hence, alternate approaches are required to constrain the multi-stage exposure/burial histories of such samples. Here, we report 28 paired analyses of ^{10}Be and ^{26}Al in boulder samples from Thule, northwest Greenland. We use numerical models of exposure and burial as well as Monte Carlo simulations to constrain glacial chronology and infer process in this Arctic region dominated by cold-based ice. We investigate three specific cases that can arise with paired nuclide data: (1) exposure ages that are coeval with deglaciation and $^{26}\text{Al}/^{10}\text{Be}$ ratios consistent with constant exposure; (2) exposure ages that pre-date deglaciation and $^{26}\text{Al}/^{10}\text{Be}$ ratios consistent with burial following initial exposure; and (3) exposure ages that pre-date deglaciation and $^{26}\text{Al}/^{10}\text{Be}$ ratios consistent with constant exposure. Most glacially-transported boulders in Thule have complex histories; some were exposed for tens of thousands of years and buried for at least hundreds of thousands of years, while others underwent only limited burial. These boulders were recycled through different generations of till over multiple glacial/interglacial cycles, likely experiencing partial or complete shielding during interglacial periods due to rotation or shallow burial by sediments. Our work demonstrates that the landscape in Thule, like many high-latitude landscapes, was shaped over long time durations and multiple glacial and interglacial periods throughout the Quaternary.

The University of Vermont

DEPARTMENT OF GEOLOGY
DELAHANTY HALL
180 COLCHESTER AVENUE
BURLINGTON, VERMONT 05405-1758
(802) 656-3396
FAX (802) 656-0045



January 28, 2016

To the Editor:

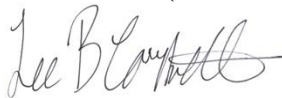
After performing a second set of revisions from two reviewers, we are resubmitting our manuscript, **Constraining Multi-Stage Exposure-Burial Scenarios for Boulders Preserved Beneath Cold-Based Glacial Ice in Thule, Northwest Greenland**, for publication in *Earth and Planetary Science Letters*.

We appreciated the additional comments from the two Reviewers who revisited the manuscript and are glad to hear that our first round of revisions was effective. During this second round, we focused on making the minor wording changes suggested and providing additional information about quantification of Al in samples. Attached, you will find a list of the reviewers' suggestions and details about how we incorporated those suggestions.

We are optimistic that these minor revisions have finished polishing the manuscript to ready it for publication. Thank you in advance for considering our revised draft.

Sincerely,

Lee Corbett (for the author team)



Department of Geology and Rubenstein School of Environment and Natural Resources
University of Vermont
180 Colchester Ave, Burlington VT 05405
Ashley.Corbett@uvm.edu
(802) 380-2344

Please note: Our responses to the reviewers can be found in red, below.

Comments from Derek Vance, Editor

Ms. Ref. No.: EPSL-D-15-00732R1

Title: Constraining multi-stage exposure-burial scenarios for boulders preserved beneath cold-based glacial ice in Thule, Northwest Greenland
Earth and Planetary Science Letters

Dear Dr. Corbett,

Thank you for the re-submission of this paper and for dealing so thoroughly with the comments of the previous reviewers. As I suggested I would in my decision letter last time, I sent the revision to two of the previous reviewers. Both of these are very happy with the revision and have only minor comments.

Please could you attend to the final points listed below on your revised manuscript, and then I will be able to accept it for publication. Given that the requested revisions are fairly minor the new version is required within 1 month.

We are glad to hear that our treatment of the first round of reviews was satisfactory. We have made the minor changes detailed below and are resubmitting a revised draft for publication. Most of our work focused on adding additional information about quantification of total Al in the samples as suggested by Reviewer #1.

Comments from Reviewer #1

The author's did a good job incorporating the suggestions, the revised manuscript is much improved and I recommend publication in EPSL for the reasons outlined in my first review. The incorporation of section 5.5 is a significant improvement and the 'AMS standard' issue is now well explained.

We thank the Reviewer for making these suggestions in the initial review and are glad to hear the revisions we made, particularly the addition of Section 5.5, improved the manuscript.

One 'misunderstanding' and remaining problem: I was not implying to produce more data, but I still would like to see ^{27}Al raw data and more details about how the ICP-OES based ^{27}Al concentrations and errors are constraint. Still no information about this, so I cannot fully recalculate the ^{26}Al ages and burial numbers. I actually would again motivate the authors to include these numbers in the supplemental table. Not much work, but important!

We are grateful to the reviewer for clarifying this point and regret the misunderstanding that occurred during the first round of revisions. We agree that ^{27}Al quantification is important and have sought to make this element of the manuscript more accessible. To the text in the methods section, we added information about which ICP-OES emission lines we used as well as statistics about the replication of Al quantification of blanks (whereas before we had reported only data for the samples). To the table in the data supplement, we added two columns that provide ICP-quantified total Al based on each of the two replicates. We think these additions, coupled with the pre-existing text, provide the necessary background for the reader to understand Al quantification and uncertainty.

This paper is going to be very helpful for many future studies. Nice work!

Comments from Reviewer #2

Based on the 'response to reviews' letter and the new manuscript itself, it is clear the authors have made an admirable effort to address and incorporate every comment from all three reviewers. I really like the revised version and find it immediately understandable from both a cosmogenic and a geomorphological point of view. The article will appeal to and be more accessible to a broader audience and be more widely cited. This version presents and reveals some of the interesting details of two nuclide analysis and interpretation in a way that can be understood by non-experts. In detail, for example, the explanation on the bottom of page 16 of the samples whose ratio suggests continuous simple exposure, but whose ages are too old in light of stratigraphic relations, is excellent.

I would like to comment and say the authors are completely correct in their assessment of the ^{26}Al data. None of their $^{26}/^{10}\text{Al}$ points is outside the realm of 'natural' $^{26}/^{10}\text{Al}$ ratios reported by many other groups. Their data is very robust.

We thank the Reviewer for the positive feedback and are happy to hear that the revisions we performed make the manuscript more accessible and relevant.

Very minor detailed comments:

p. 3 line 46 cosmic rays not cosmogenic rays.

Change made.

p. 6 line 114 I don't think the hyphen is correct here, no hyphen needed : glacially-deposited boulders.

Change made.

p. 7 line 117 ; also p. 17 line 354 I would spell it orthogneisses not orthogneises.

Change made in both locations, plus p. 5 line 85.

p. 15 line 309 I believe it is the change in dominance of obliquity (41 ka) to dominance of eccentricity (100 ka), not change in the obliquity pattern.

We have rewritten the phrase in question to read: "...when the tempo of glacial cycles changed from 41 ka to 100 ka (Raymo et al., 1997)".

Highlights:

Constraining multi-stage exposure-burial scenarios for boulders preserved beneath cold-based glacial ice in Thule, Northwest Greenland

Lee B. Corbett*^a, Paul R. Bierman^a, and Dylan H. Rood^b

*Corresponding Author: Ashley.Corbett@uvm.edu, (802) 380-2344

^aDepartment of Geology and Rubenstein School of Environment and Natural Resources, University of Vermont, Burlington, VT 05405

^bDepartment of Earth Science and Engineering, Imperial College London, South Kensington Campus, London SW7 2AZ, UK & Scottish Universities Environmental Research Centre (SUERC), East Kilbride G75 0QF, UK

- We conducted cosmogenic $^{26}\text{Al}/^{10}\text{Be}$ analysis of boulders from Thule, NW Greenland
- We utilized numerical models to constrain exposure/burial scenarios and uncertainty
- Most of the boulders have been preserved beneath cold-based, non-erosive ice
- Some boulders were exposed during Marine Isotope Stages 5e and 1
- Other boulders have longer, more complex histories spanning hundreds of ky

Revised Submission

CONSTRAINING MULTI-STAGE EXPOSURE-BURIAL SCENARIOS FOR BOULDERS
PRESERVED BENEATH COLD-BASED GLACIAL ICE IN THULE, NORTHWEST
GREENLAND

Lee B. Corbett^{*a}, Paul R. Bierman^a, and Dylan H. Rood^b

*Corresponding Author: Ashley.Corbett@uvm.edu, (802) 380-2344

^aDepartment of Geology and Rubenstein School of Environment and Natural Resources, University of Vermont, Burlington, VT 05405

^bDepartment of Earth Science and Engineering, Imperial College London, South Kensington Campus, London SW7 2AZ, UK & Scottish Universities Environmental Research Centre (SUERC), East Kilbride G75 0QF, UK

1 **Abstract**

2 Boulders and landscapes preserved beneath cold-based, non-erosive glacial ice violate
3 assumptions associated with simple cosmogenic exposure dating. In such a setting, simple single
4 isotope exposure ages over-estimate the latest period of surface exposure; hence, alternate
5 approaches are required to constrain the multi-stage exposure/burial histories of such samples.
6 Here, we report 28 paired analyses of ^{10}Be and ^{26}Al in boulder samples from Thule, northwest
7 Greenland. We use numerical models of exposure and burial as well as Monte Carlo simulations
8 to constrain glacial chronology and infer process in this Arctic region dominated by cold-based
9 ice. We investigate three specific cases that can arise with paired nuclide data: (1) exposure ages
10 that are coeval with deglaciation and $^{26}\text{Al}/^{10}\text{Be}$ ratios consistent with constant exposure; (2)
11 exposure ages that pre-date deglaciation and $^{26}\text{Al}/^{10}\text{Be}$ ratios consistent with burial following
12 initial exposure; and (3) exposure ages that pre-date deglaciation and $^{26}\text{Al}/^{10}\text{Be}$ ratios consistent
13 with constant exposure. Most glacially-transported boulders in Thule have complex histories;
14 some were exposed for tens of thousands of years and buried for at least hundreds of thousands
15 of years, while others underwent only limited burial. These boulders were recycled through
16 different generations of till over multiple glacial/interglacial cycles, likely experiencing partial or
17 complete shielding during interglacial periods due to rotation or shallow burial by sediments.
18 Our work demonstrates that the landscape in Thule, like many high-latitude landscapes, was
19 shaped over long time durations and multiple glacial and interglacial periods throughout the
20 Quaternary.

21

22 **Key words:** geochronology; cosmogenic nuclides; Polar Regions; cold-based ice; till recycling;
23 Quaternary

24 **1. Introduction**

25 *In situ* produced cosmogenic nuclides, such as ^{10}Be and ^{26}Al , are widely used to
26 reconstruct glacial histories (Balco, 2011; Fabel and Harbor, 1999). These nuclides, produced
27 predominately by nuclear spallation reactions caused by the bombardment of cosmic rays, build
28 up in rock surfaces at predictable rates over time (Lal, 1988) and can be used to make inferences
29 about surface exposure history (Granger et al., 2013). However, measurement of cosmogenic
30 nuclides in cold, high-latitude areas can yield results that are complex and challenging to
31 interpret (Briner et al., 2005). Both bedrock surfaces and boulders can yield exposure ages that
32 are older than expected, sometimes by hundreds of thousands of years (Bierman et al., 1999).
33 Rather than forming a single, normally distributed population, exposure ages from boulders in
34 polar regions often form multi-modal distributions (Marsella et al., 2000), consistent with
35 exposure during different numbers of interglacial periods as till was repeatedly reworked (Briner
36 et al., 2005; Corbett et al., 2015). When multiple nuclides with different half lives are analyzed
37 in the same sample, they can (but do not always) yield discordant exposure ages and isotopic
38 ratios indicative of at least one period of burial following initial exposure (Bierman et al., 1999).
39 Pre-deglaciation exposure ages, multi-modal age distributions, and discordant ages from
40 different isotopes are all consistent with landscapes preserved for multiple glacial/interglacial
41 cycles beneath cold-based, non-erosive ice.

42 Non-erosive glacial ice existed widely in high latitude regions in the past, including areas
43 of Greenland (Bierman et al., 2014; Håkansson et al., 2008), Antarctica (Nishiizumi et al., 1991),
44 Arctic Canada (Bierman et al., 1999; Briner et al., 2003), and Scandinavia (Stroeven et al.,
45 2002). Cold-based ice also existed in mid-latitude regions, especially at high elevations (Bierman
46 et al., 2015) and along thin ice sheet margins (Colgan et al., 2002). Since cosmic rays attenuate

47 as they pass through Earth materials at a rate controlled by density, burial by ~10 m of ice causes
48 production of nuclides by spallation to become negligible (Lal, 1988). But because bedrock and
49 boulders buried by cold-based ice are not deeply eroded, they can contain cosmogenic nuclides
50 inherited from previous periods of exposure and thus violate the primary assumption of simple
51 cosmogenic exposure dating: that the sample surface began the exposure period of interest
52 containing no cosmogenic nuclides. Constraining the history of once-glaciated bedrock surfaces
53 and boulders that have been alternately exposed and buried with little erosion requires the use of
54 multiple isotopes including a stable nuclide (^3He or ^{21}Ne) and/or radioactive nuclides (e.g. ^{10}Be ,
55 ^{26}Al , ^{36}Cl , and ^{14}C) in order to quantify the durations of exposure and burial (Bierman et al.,
56 1999; Briner et al., 2003; Briner et al., 2006; Corbett et al., 2013; Håkansson et al., 2008; Kaplan
57 et al., 2001; Marquette et al., 2004; Stroeven et al., 2002; Sugden et al., 2005).

58 Measuring at least two radioactive cosmogenic nuclides in a single sample sheds light on
59 multi-stage exposure/burial histories because the nuclides decay at different rates when the
60 sampled surface is shielded from cosmic-ray exposure (but not eroded) and nuclide production
61 ceases (Granger, 2006). Such data are typically plotted on a two-isotope diagram, where samples
62 can either overlap or fall below a pathway consistent with constant surface exposure (Klein et al.,
63 1986). Using two nuclides, a minimum total history (one period of exposure followed by one
64 period of burial) can be calculated (Fabel and Harbor, 1999), providing minimum limits of
65 exposure and burial durations (Bierman et al., 1999). However, limitations still persist even with
66 the multiple-nuclide approach since modeled histories represent non-unique inverse solutions.

67 Here, we present and analyze measurements of ^{10}Be and ^{26}Al in samples from 28
68 glacially-deposited boulders collected near Thule, northwest Greenland (Fig. 1), a long-lived
69 landscape preserved beneath non-erosive glacial ice (Corbett et al., 2015). These boulders were

70 sourced from two distinct diamict units that were deposited at different times and by different
71 bodies of ice. Our goal is to make inferences about land surface development, boulder
72 source/transport, and the history of ice cover in this cold-based ice landscape. We seek to
73 provide additional constraints on the non-unique solutions that can arise when using cosmogenic
74 nuclides at high latitude where ice is cold-based and exposure histories are often complex and
75 multi-stage. Utilizing paired cosmogenic nuclides, numerical models, and Monte Carlo
76 simulations, we provide a generalizable approach to understanding the history of cold-based ice
77 landscapes and the sediments that mantle them.

78

79 **2. Study Site, Previous Work, and Data Set**

80 Thule, northwest Greenland (~69°W, 77°N) is located on the coast at the margin of the
81 Greenland Ice Sheet, bordered on the east by TUTO Ice Dome and on the north by the Harald
82 Moltke Bræ outlet glacier (Fig. 1). Little bedrock is exposed in the study area, although Late
83 Proterozoic basin sediments of the Thule Supergroup (including shale and redbeds) crop out in
84 the areas of high topography lying to the north and northeast of Thule Air Base, close to
85 Wolstenholme Fjord (Dawes, 2006). Archaean basement orthogneisses and paragneisses are
86 exposed to the east of the study area between TUTO Ice Dome and Harald Moltke Bræ, as well
87 as across the fjord on the north side of Harald Moltke Bræ (Dawes, 2006). Previous work
88 constrained the timing of the last deglaciation to a minimum of ~10-9 cal ka BP with radiocarbon
89 ages of mollusk shells in raised marine material (Goldthwait, 1960; Morner and Funder, 1990).
90 Mollusk ages and stratigraphic analysis also suggest that Harald Moltke Bræ readvanced more
91 recently than ~10 cal ka BP, possibly in concert with the 8.2 ka cold reversal (Corbett et al.,
92 2015). Ice margins later receded inland of their current position during the mid-Holocene, as

93 constrained by radiocarbon ages of marine shells embedded in glacial shear planes (Goldthwait,
94 1960; Morner and Funder, 1990).

95 Additional work investigated the glacial history of Thule with mapping and cosmogenic
96 exposure dating. Corbett et al. (2015) documented two different surface sedimentary units: a
97 clay-rich diamict deposited by the main Greenland Ice Sheet during the last glaciation and a
98 sandy diamict deposited by a subsequent re-advance of the Harald Moltke Bræ outlet glacier
99 immediately north of Thule (Fig. 1). Although simple exposure dating with ^{10}Be was
100 complicated by the presence of nuclides inherited from past periods of exposure, Corbett et al.
101 (2015) inferred the timing of the last deglaciation to be ~ 11 ka based on the youngest ^{10}Be ages
102 from boulders in the clay-rich diamict, an age estimate supported by previous radiocarbon dating
103 of marine bivalves. The findings of Corbett et al. (2015) strongly suggest that at least some
104 boulders in the Thule area, which preserve tens of thousands of years worth of exposure history
105 and form multi-modal age distributions, contain cosmogenic nuclides inherited from previous
106 exposure due to subglacial landscape preservation beneath cold-based, non-erosive ice. Based on
107 the old simple ^{10}Be exposure ages and small 1σ analytic uncertainties (average of $2.8 \pm 0.6\%$),
108 the original dataset described in Corbett et al. (2015) is an ideal candidate for analysis of an
109 additional nuclide (^{26}Al), the results of which we present here and assess with numerical
110 modeling approaches.

111

112 **3. Methods**

113 *3.1. Sample Collection, Laboratory Preparation, and Single-Isotope Exposure Ages*

114 Samples were collected in 2011-2013 from 28 glacially deposited boulders, all of which
115 were above the post-glacial marine limit of ~ 40 -50 m (Morner and Funder, 1990). Details of

116 sample collection and processing are presented in Corbett et al. (2015). Boulder lithologies are
117 dominantly granite gneiss, likely derived from outcrops of the Archaean orthogneisses described
118 by Dawes (2006) that are exposed to the north and east of the study area. Thirteen boulders were
119 located in the clay-rich diamict unit and 15 were located in the sandy diamict unit (Table 1, Fig.
120 1).

121 We added $\sim 250 \mu\text{g}$ of ^9Be to each sample using in-house-made beryl carrier. If needed,
122 we added ^{27}Al using $1000 \mu\text{g mL}^{-1}$ SPEX Al standard. Additions of ^{27}Al carrier were optimized
123 to reach a total of $\sim 2500 \mu\text{g}$ Al in each sample based upon quantification of native ^{27}Al in
124 purified quartz. We then quantified total ^{27}Al in the samples via inductively-coupled plasma
125 optical emission spectrometry (ICP-OES) analysis of replicate aliquots removed from the
126 samples immediately following digestion (see supplemental data); these aliquots represent $\sim 2\%$
127 and 4% of the sample mass, respectively. We used two emission lines for each element (Be,
128 234.861 and 249.473 nm; and Al, 308.215 and 309.271 nm) and two internal standards (Ga and
129 Y) for all analyses. The agreement between Al estimates for the replicate analyses of process
130 blanks is $0.4 \pm 0.4 \%$ (average, 1SD, $n = 4$ sets of replicates) while the agreement between Al
131 estimates for the replicate analyses of samples is $1.1 \pm 2.9 \%$ (average, 1SD, $n = 28$ sets of
132 replicates). We use the ICP-quantified total ^{27}Al ($1824\text{-}4028 \mu\text{g}$; see supplemental data) of all
133 samples and blanks for further calculations. Since the uncertainty of our ^{27}Al quantification is
134 less than the analytic uncertainty of the AMS measurements, we did not propagate the ^{27}Al
135 quantification uncertainty into our calculation of sample ^{26}Al concentrations.

136 Isotopic ratios were measured by Accelerator Mass Spectrometry (AMS) at the Scottish
137 Universities Environmental Research Centre (Xu et al., 2015). Measured sample ratios for
138 $^{10}\text{Be}/^9\text{Be}$ (see supplemental data) are $6.6 \cdot 10^{-14}$ to $5.6 \cdot 10^{-13}$ (average analytic uncertainty $2.8 \pm$

139 0.5%, 1SD, n = 28). Ratios were normalized to the NIST standard, with an assumed $^{10}\text{Be}/^9\text{Be}$
140 ratio of $2.79 \cdot 10^{-11}$. We used a $^{10}\text{Be}/^9\text{Be}$ background ratio of $2.7 \pm 0.2 \cdot 10^{-15}$ (average, 1SD, n = 3),
141 which equates to $4.1 \pm 0.4 \cdot 10^4$ atoms of ^{10}Be , representing a 2.0 ± 0.8 % blank correction for the
142 samples (average, 1SD, n = 28). Measured sample ratios for $^{26}\text{Al}/^{27}\text{Al}$ (see supplemental data)
143 are $1.1 \cdot 10^{-13}$ to $8.8 \cdot 10^{-13}$ (average analytic uncertainty $3.5 \pm 0.8\%$, 1SD, n = 28). Ratios were
144 normalized to standard Z92-0222 with an assumed $^{26}\text{Al}/^{27}\text{Al}$ ratio of $4.11 \cdot 10^{-11}$, which is closely
145 inter-calibrated with standard KNSTD (Xu et al., 2015). We used a $^{26}\text{Al}/^{27}\text{Al}$ background ratio of
146 $8.7 \pm 3.9 \cdot 10^{-16}$ (average, 1SD, n = 4), which equates to $4.8 \pm 2.2 \cdot 10^4$ atoms of ^{26}Al , representing
147 a 0.3 ± 0.1 % blank correction for the samples (average, 1SD, n = 28). We subtracted
148 background ratios from sample ratios and propagated uncertainties in quadrature.

149 We calculated simple exposure ages using the CRONUS Earth calculator (Balco et al.,
150 2008) with calculator version 2.2 and constants version 2.2.1. We employed the northeastern
151 North American sea-level production rates of 3.93 ± 0.19 atoms $\text{g}^{-1} \text{yr}^{-1}$ for ^{10}Be and 26.54 ± 1.35
152 atoms $\text{g}^{-1} \text{yr}^{-1}$ for ^{26}Al (Balco et al., 2009) and the Lal/Stone constant production rate model and
153 scaling scheme (Lal, 1991; Stone, 2000).

154

155 *3.2. Two-Isotope Exposure and Burial Durations*

156 To perform two-isotope exposure/burial calculations, we normalized nuclide
157 concentrations to sea level using the CRONUS-determined production rates (Table 1). We
158 assume a $^{26}\text{Al}/^{10}\text{Be}$ production ratio of 6.75 (Balco et al., 2009), a ^{10}Be half-life of $1.36 \cdot 10^6$ yr
159 (Nishiizumi et al., 2007), and a ^{26}Al half-life of $7.05 \cdot 10^5$ yr (Nishiizumi, 2004). We assume no
160 nuclide production during burial by ice. Before two-isotope calculations were performed, sample
161 nuclide concentrations were corrected for the most recent period of continuous exposure (Table

162 1) based on the average ^{10}Be exposure age of the three youngest samples from this data set (10.7
163 ka; GT022, GT023, and GT055; Table 1). To perform this correction, we subtracted 10.7 ky
164 worth of surface nuclide production from each sample's ^{10}Be and ^{26}Al concentrations; this
165 correction shifts sample points downward and leftward on the two-isotope diagram, yielding
166 shorter minimum limiting exposure durations and longer minimum burial durations than if the
167 data had not been corrected. Using the corrected $^{26}\text{Al}/^{10}\text{Be}$ ratio as a filter, we modeled two-
168 isotope histories only for samples that had corrected $^{26}\text{Al}/^{10}\text{Be}$ ratios indicative of burial beyond
169 1σ analytic uncertainties ($n = 8$) and report isotopic concentrations corrected for the most recent
170 period of exposure only for these eight samples.

171 We conducted Monte Carlo simulations (10,000 models, varying ^{26}Al and ^{10}Be
172 independently and assuming a normal uncertainty distribution for each isotope concentration) for
173 the eight samples (GT014, GT015, GT016, GT019, GT021, GT036, GT054, and GT058) that
174 had $^{26}\text{Al}/^{10}\text{Be}$ ratios indicative of burial after initial exposure. For each randomly selected pair of
175 independent $^{26}\text{Al}/^{10}\text{Be}$ concentrations, we calculated minimum limiting exposure and burial
176 durations as described in Bierman et al. (1999), solving iteratively to determine the simplest
177 numerical solution (one period of exposure followed by one period of burial, Fig. 2). We then
178 used these 10,000 simulations to create probability density functions for the exposure and burial
179 duration populations (Fig. 3) and calculated a mean and a standard deviation in order to assign a
180 central tendency and an uncertainty for each sample's modeled exposure and burial durations.
181 For these eight samples, we report (Table 2) the mean exposure and burial durations, their 1σ
182 uncertainties, and the minimum total history (the sum of the initial exposure duration, the burial
183 duration, and the assumed most recent exposure duration of 10.7 ky).

184

185 *3.3. Forward Exposure/Burial Scenario Models*

186 We utilize multi-stage forward exposure/burial models to constrain possible boulder
187 histories, assuming the same production rates and half-lives described above. In these models,
188 we assume that boulders may have been exposed during one or multiple interglacial periods with
189 the low global ice volume: marine isotope stages (MIS) 15, 11, 9, and 5e (Lisiecki and Raymo,
190 2005). In scenarios involving numerous periods of exposure, we utilize incrementally increasing
191 exposure durations (2 ky increments up to 10 ky for the last period of exposure) to simulate the
192 boulder slowly making its way toward the coast via glacial transport and experiencing longer ice-
193 free periods. We use burial durations of 200 ky during MIS 14-12, 75 ky during MIS 10, 225 ky
194 during MIS 8-6, and 100 ky during MIS 4-2, based on the timing described in Lisiecki and
195 Raymo (2005). We do not include the most recent period of exposure (~10.7 ky) in these models
196 so that the modeled isotopic concentrations (at the end of MIS 2) are comparable to the corrected
197 isotopic concentrations in Thule samples for which minimum limiting exposure and burial
198 durations were calculated.

199 We also use forward models to simulate cases in which boulders experience partial
200 shielding during interglacial periods due to cover by overlying material, either because the
201 boulder was rotated (thus placing the sample surface on the bottom during prior exposure) or was
202 covered by till. For these models, we use 10 ky exposure periods alternating with 100 ky burial
203 periods. During exposure, we utilize varying nuclide production scenarios that are based on
204 portions of surface production, where 100% corresponds to no burial and full surface production.
205 Our first modeled case (60% of surface production rates) equates to burial by ~35 cm of
206 overlying rock or ~55 cm of overlying till. Our second modeled case (30% of surface production

207 rates) equates to burial by ~70 cm of rock or ~110 cm of till. The above assume a cosmic ray
208 attenuation length of 160 g cm^{-2} , a rock density of 2.7 g cm^{-3} , and a till density of 1.8 g cm^{-3} .

209

210 **4. Results**

211 For the 28 glacially-deposited boulders we sampled in the Thule area, ^{10}Be
212 concentrations are $5.2 \cdot 10^4$ to $4.3 \cdot 10^5$ atoms g^{-1} , yielding simple exposure ages of 10.6 to 77.5
213 ka; ^{26}Al concentrations are $3.7 \cdot 10^5$ to $2.2 \cdot 10^6$ atoms g^{-1} , yielding simple exposure ages of 10.7
214 to 59.0 ka (Tables 1 and 2). Exposure ages calculated with ^{10}Be and ^{26}Al are well correlated (R^2
215 = 0.95, $p < 0.01$), although ^{10}Be ages are systematically greater than ^{26}Al ages (regression slope =
216 0.72). Exposure ages from both isotopes form multi-modal age distributions with a distinct
217 young peak ~11 ka, numerous overlapping peaks ~15-30 ka, and a single older outlier (Fig. 4).
218 Measured $^{26}\text{Al}/^{10}\text{Be}$ ratios are 5.13 ± 0.14 to 8.50 ± 0.49 (average 6.85 ± 0.65 , $n = 28$, 1SD), and
219 $^{26}\text{Al}/^{10}\text{Be}$ ratios corrected for the most recent period of exposure (reported only for the eight
220 samples with $^{26}\text{Al}/^{10}\text{Be}$ ratios indicative of complex histories) are as low as 4.88 (Table 1, Fig.
221 5).

222 There is no relationship between simple exposure age and the sedimentary unit from
223 which the boulder was sourced (Table 2). Simple ^{10}Be boulder exposure ages from the clay-rich
224 diamict are 25.5 ± 17.0 ka (average, 1SD, $n = 13$) while those from the sandy diamict are $21.2 \pm$
225 5.0 ka (average, 1SD, $n = 15$), representing two populations that are not statistically
226 distinguishable ($p = 0.40$ for an unequal variance two-tailed Student's T-test). There is, however,
227 a relationship between boulder history (as reflected by the $^{26}\text{Al}/^{10}\text{Be}$ ratio) and sedimentary unit
228 (Table 1). Uncorrected boulder $^{26}\text{Al}/^{10}\text{Be}$ ratios from the clay-rich diamict are 6.55 ± 0.66
229 (average, 1SD, $n = 13$) while those from the sandy diamict are 7.11 ± 0.54 (average, 1SD, $n =$

230 15), representing two distinguishable populations ($p = 0.02$ for an unequal variance two-tailed
231 Student's T-test).

232 For the eight samples with corrected $^{26}\text{Al}/^{10}\text{Be}$ ratios indicative of burial following initial
233 exposure, we modeled exposure/burial durations and the associated uncertainties (Table 2).
234 Modeled minimum limiting exposure durations prior to burial are 11 to 96 ky (not including the
235 most recent period of exposure) and modeled minimum limiting burial durations are 88 to 627
236 ky. Minimum total histories (the sum of initial exposure duration, burial duration, and the most
237 recent exposure duration) are 111 to 734 ky. Exposure duration uncertainties as constrained by
238 Monte Carlo simulations are 1 to 4 ky, or 4 to 8% (average of 7%, 1SD) while burial duration
239 uncertainties are 55 to 112 ky, or 9 to 105% (average of 37%, 1SD). Uncertainties scale
240 inversely with modeled duration (see supplemental data).

241

242 **5. Discussion**

243 Cosmogenic data from boulders in cold-based ice regions generally fall into three
244 different categories. 1.) Samples have simple exposure ages coincident with independent
245 estimates of local deglaciation and $^{26}\text{Al}/^{10}\text{Be}$ ratios indistinguishable from continuous exposure
246 within 1σ analytic uncertainties; these samples are likely free of cosmogenic nuclides from
247 previous periods of exposure and record the timing of deglaciation. 2.) Samples have pre-
248 deglaciation simple exposure ages and $^{26}\text{Al}/^{10}\text{Be}$ ratios that fall below the constant exposure
249 pathway beyond 1σ analytic uncertainties; these samples likely experienced long durations of
250 burial (hundreds of ky) by non-erosive or weakly-erosive ice and short durations of interglacial
251 exposure. 3.) Samples have pre-deglaciation simple exposure ages but $^{26}\text{Al}/^{10}\text{Be}$ ratios that are
252 consistent with constant exposure within 1σ analytic uncertainties; these samples may have

253 experienced limited burial, but burial durations were not long enough to cause a detectable
254 change in the $^{26}\text{Al}/^{10}\text{Be}$ ratio and/or the samples were re-exposed after burial long enough to
255 increase the $^{26}\text{Al}/^{10}\text{Be}$ ratio so that it is not distinguishable from the production ratio (Bierman et
256 al., 2015). We investigate these three different cases here, all of which are represented by the
257 boulders from Thule.

258

259 *5.1. Young Exposure Ages and $^{26}\text{Al}/^{10}\text{Be}$ Ratios Indicative of Constant Exposure*

260 Deep subglacial erosion (at least several meters) can occur even in cold, high-latitude
261 areas, especially in fjord bottoms where the ice is thick and the flow is channelized (Briner et al.,
262 2009; Corbett et al., 2011; Davis et al., 1999; Hughes et al., 2012; Kaplan et al., 2001; Young et
263 al., 2011). In these areas, boulders freshly quarried from eroded bedrock surfaces yield simple
264 exposure ages that record the timing of deglaciation and $^{26}\text{Al}/^{10}\text{Be}$ ratios that overlap the constant
265 exposure pathway within 1σ analytic uncertainties.

266 In Thule, only three of the 28 samples (GT022, GT023, and GT055, all from the clay-rich
267 diamict) appear to have simple exposure ages that record the timing of deglaciation (Table 2).
268 We make this inference because these samples form their own distinct population of ages (Fig. 4)
269 and their ages agree closely with independent minimum deglaciation limits of $\sim 10\text{-}9$ cal ka BP
270 developed using radiocarbon dating of marine bivalves in the same location (Corbett et al., 2015;
271 Goldthwait, 1960; Morner and Funder, 1990). This implies that although deep glacial erosion can
272 occur on this landscape, it is spatially restricted. These three boulders suggest deglaciation at
273 10.7 ± 0.1 ka (average, 1SD, taking into account only the ^{10}Be ages) or 11.0 ± 0.5 ka (average,
274 1SD, taking into account both ^{10}Be and ^{26}Al ages).

275

276 *5.2. Old Exposure Ages and $^{26}\text{Al}/^{10}\text{Be}$ Ratios Indicative of Burial*

277 Long durations of burial by cold-based, non-erosive glacial ice cause samples to have
278 pre-deglaciation simple exposure ages and $^{26}\text{Al}/^{10}\text{Be}$ ratios inconsistent with constant exposure
279 beyond 1σ analytic uncertainties. In cold-based environments, subglacial erosion is minimal,
280 thereby preserving nuclides from previous periods of exposure and leading to surfaces that
281 reflect at least hundreds of thousands of years worth of history (Bierman et al., 1999; Corbett et
282 al., 2013). In these areas, modern landscapes are a product of development over numerous
283 glacial/interglacial cycles (Kleman and Borgstrom, 1994; Sugden and Watts, 1977).

284 In Thule, eight of the 28 samples (GT014, GT015, GT016, GT019, GT021, GT036,
285 GT054, and GT058) have old ages and $^{26}\text{Al}/^{10}\text{Be}$ ratios lower than production (assuming a
286 production ratio of 6.75; Table 2). Seven of these eight are from the clay-rich diamict, while only
287 one (GT036) is from the sandy diamict. Modeled minimum limiting exposure durations are tens
288 of ky while modeled minimum limiting burial durations are hundreds of ky (Table 2). Exposure
289 durations (including the most recent period of exposure) represent on average only $\sim 11\%$ (range
290 of 4-21%) of the total history of these samples; the small proportion of exposure is suggestive of
291 boulders that spend most of their history buried beneath non-erosive glacial ice and possibly also
292 by till during interglacial periods, experiencing only relatively brief periods of subaerial
293 exposure.

294 Results from forward models (not including the most recent period of exposure)
295 demonstrate that these eight samples preserve a range of histories. Samples GT014 and GT058,
296 which have $^{26}\text{Al}/^{10}\text{Be}$ ratios of 6.45 and 6.29, respectively, are well explained by initial exposure
297 during MIS 9 and re-exposure during MIS5e (Fig. 6). Samples GT015 and GT016 have lower
298 $^{26}\text{Al}/^{10}\text{Be}$ ratios, necessitating more burial and hence a scenario including more

299 glacial/interglacial cycles: possibly exposure during MIS 15, 11, 9, and 5e, with burial between
300 (Fig. 6). Samples GT019, GT036, and GT054 have low $^{26}\text{Al}/^{10}\text{Be}$ ratios but also low
301 concentrations of both isotopes, measurements not well explained by scenarios involving cyclic
302 exposure and burial. Rather, these samples may be explained by a scenario in which the boulders
303 were initially exposed during an early interglacial period (e.g., MIS 11) and then remained
304 completely buried (by ice during glacial periods and till during interglacial periods) until the
305 Holocene (Fig. 6). Significantly longer-duration scenarios (at least a total of 734 ky, but likely
306 much greater) are needed to explain the data from sample GT021, which has a low $^{26}\text{Al}/^{10}\text{Be}$
307 ratio and high isotopic concentrations; this boulder could have been repeatedly exposed and
308 buried many times over much of the Quaternary period. Because there is less constraint on the
309 behavior of the Greenland Ice Sheet during the earlier part of the Quaternary, and because so
310 many possible scenarios could explain the location of sample GT021 on the two-isotope
311 diagram, we do not attempt to fit this data point with a specific forward model. Rather, we
312 suggest that this boulder likely preserves inherited nuclides from before the mid-Pleistocene
313 transition, when the tempo of glacial cycles changed from 41 ka to 100 ka (Raymo et al., 1997).

314

315 *5.3. Old Exposure Ages and $^{26}\text{Al}/^{10}\text{Be}$ Ratios Indicative of Constant Exposure*

316 Different scenarios can lead to samples that have pre-deglaciation simple exposure ages
317 and $^{26}\text{Al}/^{10}\text{Be}$ ratios consistent with constant exposure within 1σ analytic uncertainties. One
318 possibility is that the land surface on which the boulder resides has been constantly exposed as a
319 nunatak and never buried (Roberts et al., 2009; Stone et al., 1998). A second possibility is that
320 the landscape was buried by ice in the past following initial exposure, but burial was short
321 enough to not cause a detectable decrease in the $^{26}\text{Al}/^{10}\text{Be}$ ratio (Bierman et al., 2015).

322 Numerical models demonstrate that relatively short durations of burial, especially when
323 followed by re-exposure, are insufficient to result in a $^{26}\text{Al}/^{10}\text{Be}$ ratio distinguishable from the
324 constant exposure case at 1σ . Assuming a 10 ky period of exposure is followed by a 100 ky
325 period of burial and subsequent Holocene exposure, a history consistent with exposure during
326 MIS 5e and 1 and burial between, the resulting $^{26}\text{Al}/^{10}\text{Be}$ ratio is 6.59. Applying an uncertainty
327 of 4.5% to the $^{26}\text{Al}/^{10}\text{Be}$ ratio (the average ratio uncertainty of the Thule data set), the resulting
328 ratio of 6.59 is indistinguishable from 6.75 even though the surface spent over 80% of its history
329 buried. In this case, the $^{26}\text{Al}/^{10}\text{Be}$ system is unable to distinguish boulders that experienced
330 exposure during both MIS 5e and 1 from those that only experienced exposure during MIS 1.
331 The inability to detect relatively short periods of burial is partly because the $^{26}\text{Al}/^{10}\text{Be}$ ratio
332 uncertainty is greater than either of the single-isotope uncertainties (Gillespie and Bierman,
333 1995) and partly because isotopic concentrations (and hence the $^{26}\text{Al}/^{10}\text{Be}$ ratio) are more
334 sensitive to exposure than burial due to the long half lives of these nuclides in comparison to the
335 burial times. The relatively low concentrations of nuclides investigated in this study may
336 represent an additional challenge for discerning short burial durations since the analytic
337 uncertainty is more likely to overshadow small changes in nuclide concentrations caused by
338 limited burial duration.

339 In Thule, 17 of the 28 samples have simple exposure ages older than expected, but
340 $^{26}\text{Al}/^{10}\text{Be}$ ratios consistent with constant surface exposure. Only three of these 17 are from the
341 clay-rich diamict; the remaining 14 are from the sandy diamict. Based on several lines of
342 evidence, we conclude that these boulders are not indicative of constant exposure despite what
343 their $^{26}\text{Al}/^{10}\text{Be}$ ratios suggest. Because the sandy diamict stratigraphically overlies both the clay-
344 rich diamict (deposited ~ 10.7 ka based on the three youngest boulders) and marine sediments

345 (dated to ~10 cal ka BP with radiocarbon, Corbett et al. (2015)), it cannot have been deposited
346 prior to the earliest Holocene. Rather, the boulders that record pre-deglaciation exposure ages,
347 but have $^{26}\text{Al}/^{10}\text{Be}$ ratios indicative of constant exposure, were likely exposed during MIS 5e,
348 when global ice volume was low (Lisiecki and Raymo, 2005) and Greenland's coastal areas were
349 ice-free (Otto-Bliesner et al., 2006), then buried and minimally eroded until the onset of MIS 1
350 when they were re-exposed.

351

352 *5.4. Till Recycling*

353 Because our data indicate that most of the Thule boulders have been preserved
354 subglacially, it is likely that the boulders we sampled are part of till units that have been
355 repeatedly reworked and recycled. These boulders (primarily gneiss), which do not match the
356 local bedrock (weakly metamorphosed basin sediments), were likely sourced to the east of the
357 study area where Archaean basement orthogneisses are exposed (Dawes, 2006), although we are
358 unable to constrain the transport distance since the subglacial extent of these basement rocks is
359 unknown. These boulders may have been incorporated into till during one or numerous previous
360 interglacial periods, slowly progressing coastward in flowing ice over time.

361 If the boulders in Thule have indeed been assimilated into different generations of till, it
362 is likely that the surfaces we sampled were partially shielded during previous interglacial
363 periods, either because they were buried beneath other sediments or because the boulders rotated
364 and the surfaces we sampled were on the side or bottom during the past. In the case of partial
365 shielding during periods of exposure, the path taken through the two-isotope diagram compresses
366 leftward since cosmogenic nuclides form at lesser rates than in the absence of shielding (Fig. 7).
367 This overall leftward compression allows a larger number of exposure/burial cycles to occur

368 before a given ^{10}Be concentration is reached than in the absence of shielding. Hence, if multiple
369 samples have similar ^{10}Be concentrations, those that experienced partial shielding during periods
370 of exposure have also experienced a larger total number of exposure/burial cycles, leading to
371 longer burial durations and lower $^{26}\text{Al}/^{10}\text{Be}$ ratios than those that experienced no shielding (Fig.
372 7). Therefore, variable levels of shielding reflecting rotated or partially buried boulders in
373 reworked till may at least partially explain the range of observed $^{26}\text{Al}/^{10}\text{Be}$ ratios.

374 The extent and patterns of till recycling (as recorded by $^{26}\text{Al}/^{10}\text{Be}$ ratio) appear to be
375 related to the sedimentary unit from which the boulders were sourced, with the clay-rich diamict
376 having been deposited by the main Greenland Ice Sheet during the last glaciation and the sandy
377 diamict having been deposited by an early Holocene re-advance of Harald Moltke Bræ (Corbett
378 et al., 2015). The population of 13 boulders from the clay-rich diamict includes three boulders
379 with young ages and continuous exposure, seven boulders with old ages and complex history,
380 and only one boulder with an old age but a $^{26}\text{Al}/^{10}\text{Be}$ ratio indistinguishable from constant
381 exposure. Therefore, this unit appears to contain boulders recording heterogeneous processes,
382 representing either no or significant recycling with little middle ground, possibly reflecting a
383 wider source area and less erosive ice. Conversely, the population of 15 boulders from the sandy
384 diamict includes one boulder with an old age and complex history and 14 boulders with old ages
385 but $^{26}\text{Al}/^{10}\text{Be}$ ratios indistinguishable from constant exposure. Therefore, this unit appears more
386 homogeneous and the boulders record shorter total near-surface histories and less burial, possibly
387 reflecting more erosive ice in the outlet glacier.

388

389

390

391 5.5. $^{26}\text{Al}/^{10}\text{Be}$ Production Ratio

392 A significant limitation in the ability to understand complex exposure histories with a
393 multi-isotope approach lies in the uncertainty of how the $^{26}\text{Al}/^{10}\text{Be}$ production ratio varies over
394 space. Although a production ratio of 6.75 is used in most calculations (Balco et al., 2008),
395 recent work suggests that the production ratio is itself dependent on latitude and elevation.
396 Actual $^{26}\text{Al}/^{10}\text{Be}$ production ratios may be greater than 6.75, with hypothesized values ranging as
397 high as ~ 7.3 , because each isotope's production rate scales differently with altitude and latitude
398 (Argento et al., 2013; Argento et al., 2015; Borchers et al., 2015).

399 The $^{26}\text{Al}/^{10}\text{Be}$ ratios we report from Thule could be consistent with a higher than
400 currently accepted production ratio. Eleven of the 28 measured $^{26}\text{Al}/^{10}\text{Be}$ ratios exceed 6.75 by
401 more than 1σ (Table 1), compared to the four samples (16% of the population) we would expect
402 based on measurement uncertainty. If we instead assume a production ratio of 7.16 (the median
403 value of high latitude, low elevation CRONUS calibration samples reported in Argento et al.
404 (2013)), only three of our 28 samples exceed the production ratio by more than 1σ and one
405 (GT039) exceeds it by more than 2σ (Table 1), similar to what would be expected given the
406 analytic precision of our data. Although systematic measurement error could also contribute to
407 high $^{26}\text{Al}/^{10}\text{Be}$ ratios, with ICP-OES quantification of total Al being the most likely source
408 (Bierman and Caffee, 2002; Fujioka et al., 2015), we think this is unlikely since we do not see
409 this trend for lower-latitude samples processed in our laboratory.

410 The assumed $^{26}\text{Al}/^{10}\text{Be}$ production ratio has important implications for determining which
411 samples experienced a multi-stage history and for modeling those histories. Assuming a higher
412 $^{26}\text{Al}/^{10}\text{Be}$ production ratio results in fewer samples with simple exposure histories and a greater
413 number of samples with histories indicative of burial (Fig. 8). Although the $^{26}\text{Al}/^{10}\text{Be}$ production

414 ratio has little impact on modeled minimum limiting exposure duration, it has a pronounced
415 impact on modeled minimum limiting burial duration (Fig. 8). Sensitivity analysis for a
416 representative sample in our dataset (GT016) demonstrates that modeled minimum limiting
417 burial duration increases linearly with $^{26}\text{Al}/^{10}\text{Be}$ production ratio, with an additional 29 ky of
418 burial added for each 0.1 increment of $^{26}\text{Al}/^{10}\text{Be}$ production ratio. More closely constraining the
419 variability of the $^{26}\text{Al}/^{10}\text{Be}$ production ratio over space is an important direction for future work
420 since it has significant implications for detecting and quantifying burial with the two-isotope
421 approach.

422

423 **6. Conclusions**

424 The landscape in Thule, northwest Greenland, preserves a long record of heterogeneous
425 subglacial processes. A small number of the boulders we sampled (three of 28) were sourced
426 from areas deeply eroded during the last glacial period and their simple exposure ages suggest
427 deglaciation of the landscape ~ 10.7 ka, consistent with radiocarbon age control. Other boulders
428 (eight of 28) are indicative of ineffective subglacial erosion, yielding old simple exposure ages,
429 $^{26}\text{Al}/^{10}\text{Be}$ ratios indicative of burial following initial exposure, and modeled total histories of
430 hundreds of ky. These boulders likely experienced initial exposure during MIS9 or an earlier
431 interglacial period and record an exposure/burial history spanning at least several
432 interglacial/glacial cycles. Finally, most boulders (17 of 28) have old simple exposure ages that
433 pre-date deglaciation and $^{26}\text{Al}/^{10}\text{Be}$ ratios indistinguishable from constant exposure. These
434 boulders have only experienced limited burial, suggesting that they were initially exposed during
435 MIS 5e and re-exposed during MIS 1. Boulders from the clay-rich diamict unit deposited by the
436 main Greenland Ice Sheet have nuclide concentrations indicative of either no or significant

437 burial, whereas boulders from the sandy diamict unit deposited by a subsequent outlet glacier re-
438 advance have nuclide concentrations largely suggestive of limited burial durations. The boulders
439 we sampled come from till units that have likely been recycled but not deeply eroded several or
440 many times over the Quaternary, with boulders sometimes experiencing partial or complete
441 shielding during interglacial periods, leading to the range in exposure/burial scenarios we infer.
442 Together these data reinforce the heterogeneity of subglacial processes and support the use of
443 multi-nuclide approaches for studying glacial history in cold-based ice environments.

Acknowledgements

Support for this research was provided by a National Science Foundation Doctoral Dissertation Research Improvement Grant (BCS-1433878), the Geological Society of America Quaternary Geology and Geomorphology Division J. Hoover Mackin Award, an International Association of Geochemistry Student Research Grant, the Rubenstein School of Environment and Natural Resources at University of Vermont, a Dartmouth College Graduate Alumni Research Award, and NSF ARC-102319. Field support was provided by CH2MHILL, particularly J. Hurley and K. Derry. We thank G.E. Lasher and E. Osterberg for assistance during fieldwork, as well as J. Schaefer and two anonymous reviewers for improving the manuscript.

References

- Argento, D., Reedy, R., Stone, J., 2013. Modeling the earth's cosmic radiation. *Nuclear Instruments and Methods in Physics Research B* 294, 464-469.
- Argento, D., Stone, J., Reedy, R., O'Brien, K., 2015. Physics-based modeling of cosmogenic nuclides part II- Key aspects of in-situ cosmogenic nuclide production. *Quaternary Geochronology* 26, 44-55.
- Balco, G., 2011. Contributions and unrealized potential contributions of cosmogenic-nuclide exposure dating to glacier chronology, 1990-2010. *Quaternary Science Reviews* 30, 3-27.
- Balco, G., Briner, J., Finkel, R., Rayburn, J., Ridge, J., Schaefer, J., 2009. Regional beryllium-10 production rate calibration for late-glacial northeastern North America. *Quaternary Geochronology* 4, 93-107.
- Balco, G., Stone, J., Lifton, N., Dunai, T., 2008. A complete and easily accessible means of calculating surface exposure ages or erosion rates from ^{10}Be and ^{26}Al measurements. *Quaternary Geochronology* 3, 174-195.
- Bierman, P., Caffee, M., 2002. Cosmogenic exposure and erosion history of Australian bedrock landforms. *Bulletin of the Geological Society of America* 114, 787-803.
- Bierman, P., Corbett, L., Graly, J., Neumann, T., Lini, A., Crosby, B., Rood, D., 2014. Preservation of a preglacial landscape under the center of the Greenland Ice Sheet. *Science* 344, 402-405.
- Bierman, P., Davis, P., Corbett, L., Lifton, N., 2015. Cold-based, Laurentide ice covered New England's highest summits during the Last Glacial Maximum. *Geology*
DOI:10.1130/G37225.1.
- Bierman, P., Marsella, K., Patterson, C., Davis, P., Caffee, M., 1999. Mid-Pleistocene cosmogenic minimum-age limits for pre-Wisconsinan glacial surfaces in southwestern Minnesota and southern Baffin Island: a multiple nuclide approach. *Geomorphology* 27, 25-39.
- Borchers, B., Marrero, S., Balco, G., Caffee, M., Goehring, B., Lifton, N., Nishiizumi, K., Phillips, F., Schaefer, J., Stone, J., 2015. Geological calibration of spallation production rates in the CRONUS-Earth project. *Quaternary Geochronology*
<http://dx.doi.org/10.1016/j.quageo.2015.01.009>.
- Briner, J., Bini, A., Anderson, R., 2009. Rapid early Holocene retreat of a Laurentide outlet glacier through an Arctic fjord. *Nature Geoscience* 2, 496-499.
- Briner, J., Miller, G., Davis, P., Bierman, P., Caffee, M., 2003. Last Glacial Maximum ice sheet dynamics in Arctic Canada inferred from young erratics perched on ancient tors. *Quaternary Science Reviews* 22, 437-444.
- Briner, J., Miller, G., Davis, P., Finkel, R., 2005. Cosmogenic exposure dating in arctic glacial landscapes: implications for the glacial history of northeastern Baffin Island, Arctic Canada. *Canadian Journal of Earth Sciences* 42, 67-84.
- Briner, J., Miller, G., Davis, P., Finkel, R., 2006. Cosmogenic radionuclides from fjord landscapes support differential erosion by overriding ice sheets. *Geological Society of America Bulletin* 118, 406-420.
- Colgan, P., Bierman, P., Mickelson, D., Caffee, M., 2002. Variation in glacial erosion near the southern margin of the Laurentide Ice Sheet, south-central Wisconsin, USA: Implications

- for cosmogenic dating of glacial terrains. *Geological Society of America Bulletin* 114, 1581-1591.
- Corbett, L., Bierman, P., Graly, J., Neumann, T., Rood, D., 2013. Constraining landscape history and glacial erosivity using paired cosmogenic nuclides in Upernavik, northwest Greenland. *Geological Society of America Bulletin* 125, 1539-1553.
- Corbett, L., Bierman, P., Lasher, G., Rood, D., 2015. Landscape chronology and glacial history in Thule, northwest Greenland. *Quaternary Science Reviews* 109, 57-67.
- Corbett, L., Young, N., Bierman, P., Briner, J., Neumann, T., Graly, J., Rood, D., 2011. Paired bedrock and boulder ^{10}Be concentrations resulting from early Holocene ice retreat near Jakobshavn Isfjord, western Greenland. *Quaternary Science Reviews* 30, 1739-1749.
- Davis, P., Bierman, P., Marsella, K., Caffee, M., Southon, J., 1999. Cosmogenic analysis of glacial terrains in the eastern Canadian Arctic: a test for inherited nuclides and the effectiveness of glacial erosion. *Annals of Glaciology* 28.
- Dawes, P., 2006. Geological map of Greenland, 1:500,000, Thule, Sheet 5, Geological Survey of Denmark and Greenland Map Series 2. Geological Survey of Denmark and Greenland, Danish Ministry of the Environment.
- Fabel, D., Harbor, J., 1999. The use of in-situ produced cosmogenic radionuclides in glaciology and glacial geomorphology. *Annals of Glaciology* 28, 103-110.
- Fujioka, T., Fink, D., Mifsud, C., 2015. Towards improvement of aluminium assay in quartz for in situ cosmogenic ^{26}Al analysis at ANSTO. *Nuclear Instruments and Methods in Physics Research Section B: Beam Interactions with Materials and Atoms* 361, 346-353.
- Gillespie, A., Bierman, P., 1995. Precision of terrestrial exposure ages and erosion rates estimated from analysis of cosmogenic isotopes produced *in situ*. *Journal of Geophysical Research* 100, 24,637-624,649.
- Goldthwait, R., 1960. Study of ice cliff in Nunatarssuaq, Greenland. U.S. Army Snow, Ice, and Permafrost Research Establishment Technical Report 39, 106 p.
- Granger, D., 2006. A review of burial dating methods using ^{26}Al and ^{10}Be . *Geological Society of America Special Papers* 415, 1-16.
- Granger, D., Lifton, N., Willenbring, J., 2013. A cosmic trip: 25 years of cosmogenic nuclides in geology. *Geological Society of America Bulletin* 125, 1379-1402.
- Håkansson, L., Alexanderson, H., Hjort, C., Moller, P., Briner, J., Aldahan, A., Possnert, G., 2008. Late Pleistocene glacial history of Jameson Land, central East Greenland, derived from cosmogenic ^{10}Be and ^{26}Al exposure dating. *Boreas* 38, 244-260.
- Hughes, A., Rainsley, E., Murray, T., Fogwill, C., Schnabel, C., Xu, S., 2012. Rapid response of Helheim Glacier, southeast Greenland, to early Holocene climate warming. *Geology* 40, 427-430.
- Kaplan, M., Miller, G., Steig, E., 2001. Low-gradient outlet glaciers (ice streams?) drained the Laurentide ice sheet. *Geology* 29, 343-346.
- Klein, J., Giegengack, R., Middleton, R., Sharma, P., Underwood, J., Weeks, R., 1986. Revealing histories of exposure using *in situ* produced ^{26}Al and ^{10}Be in Libyan desert glass. *Radiocarbon* 28, 547-555.
- Kleman, J., Borgstrom, I., 1994. Glacial land forms indicative of a partly frozen bed. *Journal of Glaciology* 40, 255-264.
- Lal, D., 1988. In situ-produced cosmogenic isotopes in terrestrial rocks. *Annual Review of Earth and Planetary Sciences* 16, 355-388.

- Lal, D., 1991. Cosmic ray labeling of erosion surfaces: in situ nuclide production rates and erosion models. *Earth and Planetary Science Letters* 104, 424-439.
- Lisiecki, L., Raymo, M., 2005. A Plio-Pleistocene stack of 57 globally distributed benthic ^{18}O records. *Paleoceanography* 20, 522–533.
- Marquette, G., Gray, J., Gosse, J., Courchesne, F., Stockli, L., Macpherson, G., Finkel, R., 2004. Felsenmeer persistence under non-erosive ice in the Torngat and Kaumajet mountains, Quebec and Labrador, as determined by soil weathering and cosmogenic nuclide exposure dating. *Canadian Journal of Earth Sciences* 41, 19-38.
- Marsella, K., Bierman, P., Davis, P., Caffee, M., 2000. Cosmogenic ^{10}Be and ^{26}Al ages for the last glacial maximum, eastern Baffin Island, Arctic Canada. *Geological Society of America Bulletin* 112, 1296-1312.
- Morner, N., Funder, S., 1990. C-14 dating of samples collected during the NORDQUA 86 expedition, and notes on the marine reservoir effect. *Meddelelser om Gronland* 22, 57-63.
- Nishiizumi, K., 2004. Preparation of ^{26}Al AMS standards. *Nuclear Instruments and Methods in Physics Research Section B: Beam Interactions with Materials and Atoms* 223, 388-392.
- Nishiizumi, K., Imamura, M., Caffee, M., Southon, J., Finkel, R., McAninch, J., 2007. Absolute calibration of ^{10}Be AMS standards. *Nuclear Instruments and Methods in Physics Research Section B: Beam Interactions with Materials and Atoms* 258, 403-413.
- Nishiizumi, K., Kohl, C., Arnold, J., Klein, J., Fink, D., Middleton, R., 1991. Cosmic ray produced ^{10}Be and ^{26}Al in Antarctic rocks: exposure and erosion history. *Earth and Planetary Science Letters* 104, 440-454.
- Otto-Bliesner, B., Marshall, S., Overpeck, J., Miller, G., Hu, A., 2006. Simulating Arctic climate warmth and icefield retreat in the last interglaciation. *Science* 311, 1751-1753.
- Raymo, M., Oppo, D., Curry, W., 1997. The mid-Pleistocene climate transition: A deep sea carbon isotopic perspective. *Paleoceanography* 12, 546-559.
- Roberts, D., Long, A., Schnabel, C., Davies, B., Xu, S., Simpson, M., Huybrechts, P., 2009. Ice sheet extent and early deglacial history of the southwestern sector of the Greenland Ice Sheet. *Quaternary Science Reviews* 28, 2760-2773.
- Stone, J., 2000. Air pressure and cosmogenic isotope production. *Journal of Geophysical Research* 105, 23753-23759.
- Stone, J., Ballantyne, C., Fifield, L., 1998. Exposure dating and validation of periglacial weathering limits, northwest Scotland. *Geology* 26, 587-590.
- Stroeven, A., Fabel, D., Hattestrand, C., Harbor, J., 2002. A relict landscape in the centre of Fennoscandian glaciation: cosmogenic radionuclide evidence of tors preserved through multiple glacial cycles. *Geomorphology* 44, 145-154.
- Sugden, D., Balco, G., Cowdery, S., Stone, J., Sass III, L., 2005. Selective glacial erosion and weathering zones in the coastal mountains of Marie Byrd Land, Antarctica. *Geomorphology* 67, 317-334.
- Sugden, D., Watts, S., 1977. Tors, felsenmeer, and glaciation in northern Cumberland Peninsula, Baffin Island. *Canadian Journal of Earth Sciences* 14, 2817-2823.
- Xu, S., Freeman, S., Rood, D., Shanks, R., 2015. Decadal ^{10}Be , ^{26}Al and ^{36}Cl QA measurements on the SUERC 5 MV accelerator mass spectrometer. *Nuclear Instruments and Methods Section B: Beam Interactions with Materials and Atoms* 361, 39-42.

Young, N., Briner, J., Stewart, H., Axford, Y., Csatho, B., Rood, D., Finkel, R., 2011. Response of Jakobshavn Isbrae, Greenland, to Holocene climate change. *Geology* 39, 131-134.

Table Captions

Table 1. Sample collection information and isotopic data from 28 glacially-deposited boulders.

Table 2. Age data from 28 glacially-deposited boulders.

Figure Captions

Figure 1. Location of the study site. Panel A shows the location of Thule in northwest Greenland. Panel B shows the Thule region with places described in the text. Panel C shows the location of the 28 boulder samples collected for analysis of cosmogenic $^{26}\text{Al}/^{10}\text{Be}$, with the white dashed line denoting the contact between the two diamict units described in the text.

Figure 2. Example of Monte Carlo simulations for sample GT016. Each of the 10,000 simulations (black dots) indicates an iterative numerical solution of one period of exposure followed by one period of burial that explains the observed isotopic concentrations.

Figure 3. Example probability density functions of 10,000 exposure durations and 10,000 burial durations for sample GT016. We used these populations to calculate the mean and standard deviation of simulated exposure and burial durations for each sample.

Figure 4. Probability density functions for ^{10}Be (top panel) and ^{26}Al (bottom panel) simple exposure ages of 28 boulder samples. Thin gray lines indicate the probability of each individual sample; thick black line indicates the summed probability for all samples.

Figure 5. Measured $^{26}\text{Al}/^{10}\text{Be}$ ratios plotted against ^{10}Be concentrations for sea level normalized values. Top panel shows all samples, with one sample (GT039) omitted for visibility because of its high ratio ($n = 27$, 1σ error bars). Bottom panel shows only the samples that have been numerically modeled for exposure/burial ($n = 8$), with concentrations and ratios that have been corrected for the most recent period of exposure (black dots, 1σ error bars) and original uncorrected values (gray dots); see Figures 6 and 7 for sample names. Thick black line shows the constant exposure pathway. Dotted lines show erosion pathways of 25, 10, 5, 2, 1, 0.5, 0.2, and 0.1 m Ma^{-1} , from left to right. Black triangles show secular equilibrium endpoints for erosion scenarios as well as the constant exposure scenario. Burial paths are shown with thin lines, and burial isochrones (0.5, 1.0, and 1.5 Ma, from top to bottom) are shown with thin dashed lines.

Figure 6. Two-isotope diagram as described in Fig. 5. Thick colored lines show isotopic evolution resulting from various exposure/burial scenarios. We assume that exposure durations increase incrementally with each subsequent period of exposure and we utilize burial durations that reflect the chronology described in Lisiecki and Raymo (2005). Black dots show the Thule samples that have been corrected for the most recent period of exposure; numbers indicate the sample number, error bars are 1σ .

Figure 7. Two-isotope diagram as described in Fig. 5. Thick colored lines show isotopic evolution over alternate periods of exposure (10 ky) and burial (100 ky), with various levels of shielding during periods of exposure to simulate till cover or boulder rotation. Black dots show the Thule samples that have been corrected for the most recent period of exposure; numbers indicate the sample number, error bars are 1σ .

Figure 8. Sensitivity analysis investigating the effect of $^{26}\text{Al}/^{10}\text{Be}$ production ratio on inferred boulder histories using seven different production ratios: 6.75, 6.85, 6.95, 7.05, 7.15, 7.25, and 7.35. Top two panels show modeled minimum limiting exposure and burial durations for a representative sample in the dataset (GT016), with error bars showing $\pm 1\sigma$ as derived by Monte Carlo analysis. Bottom panel shows the dataset as a whole and inferences regarding how many samples are above, indistinguishable from, or below the production ratio based on 1σ $^{26}\text{Al}/^{10}\text{Be}$ analytic uncertainties. Gray bars show possible $^{26}\text{Al}/^{10}\text{Be}$ production ratios from recent studies.

Figure_1_HighRes

[Click here to download Figure \(high-resolution\): Corbett_Figure1_HighRes.tif](#)

Figure_2_HighRes

[Click here to download Figure \(high-resolution\): Corbett_Figure2_HighRes.tif](#)

Figure_3_HighRes

[Click here to download Figure \(high-resolution\): Corbett_Figure3_HighRes.tif](#)

Figure_4_HighRes

[Click here to download Figure \(high-resolution\): Corbett_Figure4_HighRes.tif](#)

Figure_5_HighRes

[Click here to download Figure \(high-resolution\): Corbett_Figure5_HighRes.tif](#)

Figure_6_HighRes

[Click here to download Figure \(high-resolution\): Corbett_Figure6_HighRes.tif](#)

Figure_7_HighRes

[Click here to download Figure \(high-resolution\): Corbett_Figure7_HighRes.tif](#)

Figure_8_HighRes

[Click here to download Figure \(high-resolution\): Corbett_Figure8_HighRes.tif](#)

Sample Name ^a	Sed. Unit ^b	Latitud (°N)	Longitud (°E)	Elevatio (m a.s.l.)	Measured Values ^c					Correc
					¹⁰ Re (atoms g ⁻¹)	1σ ¹⁰ Re Unc. (atoms g ⁻¹)	²⁶ Al (atoms g ⁻¹)	1σ ²⁶ Al (atoms g ⁻¹)	²⁶ Al/ ¹⁰ Re Ratio (1σ)	¹⁰ Re (atoms g ⁻¹)
GT014	C	76.54578	-68.15783	350	1.33 x 10 ⁵	4.22 x 10 ³	8.78 x 10 ⁵	2.84 x 10 ⁴	6.58 ± 0.30	4.84 x 10 ⁴
GT015	C	76.55843	-68.64975	276	1.60 x 10 ⁵	4.01 x 10 ³	9.95 x 10 ⁵	4.81 x 10 ⁴	6.20 ± 0.34	7.67 x 10 ⁴
GT016	C	76.55745	-68.71192	252	1.48 x 10 ⁵	3.87 x 10 ³	8.94 x 10 ⁵	2.53 x 10 ⁴	6.04 ± 0.23	6.84 x 10 ⁴
GT018	C	76.54552	-68.61322	251	1.54 x 10 ⁵	4.67 x 10 ³	1.03 x 10 ⁶	2.74 x 10 ⁴	6.64 ± 0.27	---
GT019	C	76.55382	-68.54360	178	1.12 x 10 ⁵	2.44 x 10 ³	6.72 x 10 ⁵	1.99 x 10 ⁴	6.01 ± 0.22	5.00 x 10 ⁴
GT021	C	76.54702	-68.07298	314	4.33 x 10 ⁵	8.20 x 10 ³	2.22 x 10 ⁶	4.38 x 10 ⁴	5.13 ± 0.14	2.68 x 10 ⁵
GT022 ^(R)	C	76.55833	-68.19445	358	6.45 x 10 ⁴	1.99 x 10 ³	4.39 x 10 ⁵	1.75 x 10 ⁴	6.79 ± 0.34	---
GT023 ^(R)	C	76.56945	-68.24887	346	6.30 x 10 ⁴	2.15 x 10 ³	4.71 x 10 ⁵	1.94 x 10 ⁴	7.47 ± 0.40	---
GT027	S	76.55336	-68.39177	175	1.37 x 10 ⁵	3.45 x 10 ³	9.80 x 10 ⁵	2.80 x 10 ⁴	7.16 ± 0.27	---
GT030	S	76.55168	-68.39473	171	1.13 x 10 ⁵	2.79 x 10 ³	7.81 x 10 ⁵	2.24 x 10 ⁴	6.89 ± 0.26	---
GT035	S	76.55843	-68.45382	71	1.03 x 10 ⁵	2.36 x 10 ³	7.30 x 10 ⁵	2.19 x 10 ⁴	7.08 ± 0.27	---
GT036	S	76.55791	-68.44873	77	1.06 x 10 ⁵	3.10 x 10 ³	6.32 x 10 ⁵	1.93 x 10 ⁴	5.94 ± 0.25	5.45 x 10 ⁴
GT038	S	76.55983	-68.42910	67	5.35 x 10 ⁴	1.65 x 10 ³	3.72 x 10 ⁵	1.66 x 10 ⁴	6.95 ± 0.38	---
GT039	S	76.56069	-68.42268	74	5.22 x 10 ⁴	1.66 x 10 ³	4.44 x 10 ⁵	2.14 x 10 ⁴	8.50 ± 0.49	---
GT040	S	76.56132	-68.42116	62	8.93 x 10 ⁴	4.24 x 10 ³	6.85 x 10 ⁵	2.32 x 10 ⁴	7.67 ± 0.45	---
GT042	S	76.55457	-68.38605	138	1.21 x 10 ⁵	2.78 x 10 ³	8.47 x 10 ⁵	2.46 x 10 ⁴	7.02 ± 0.26	---
GT043	S	76.55338	-68.39169	175	1.33 x 10 ⁵	3.55 x 10 ³	9.25 x 10 ⁵	4.36 x 10 ⁴	6.95 ± 0.38	---
GT044	S	76.55151	-68.39625	185	8.31 x 10 ⁴	2.08 x 10 ³	5.91 x 10 ⁵	2.17 x 10 ⁴	7.11 ± 0.32	---
GT049	S	76.57150	-68.52433	198	1.28 x 10 ⁵	3.19 x 10 ³	9.16 x 10 ⁵	3.72 x 10 ⁴	7.13 ± 0.34	---
GT050	S	76.57030	-68.51962	198	9.08 x 10 ⁴	2.40 x 10 ³	6.27 x 10 ⁵	2.60 x 10 ⁴	6.90 ± 0.34	---
GT051	S	76.56734	-68.51293	195	1.08 x 10 ⁵	2.56 x 10 ³	8.09 x 10 ⁵	2.30 x 10 ⁴	7.49 ± 0.28	---
GT052	S	76.56478	-68.50867	187	1.17 x 10 ⁵	2.92 x 10 ³	8.34 x 10 ⁵	3.77 x 10 ⁴	7.10 ± 0.37	---
GT053	S	76.56400	-68.50716	180	9.51 x 10 ⁴	2.15 x 10 ³	6.37 x 10 ⁵	1.95 x 10 ⁴	6.70 ± 0.26	---
GT054	C	76.55590	-68.57046	183	9.27 x 10 ⁴	3.10 x 10 ³	5.66 x 10 ⁵	2.11 x 10 ⁴	6.11 ± 0.31	3.30 x 10 ⁴
GT055 ^(R)	C	76.56046	-68.54910	201	5.49 x 10 ⁴	2.05 x 10 ³	4.09 x 10 ⁵	1.74 x 10 ⁴	7.46 ± 0.42	---
GT056	C	76.58178	-68.58881	324	1.29 x 10 ⁵	3.50 x 10 ³	9.09 x 10 ⁵	2.95 x 10 ⁴	7.05 ± 0.30	---
GT057	C	76.53712	-68.41935	143	1.29 x 10 ⁵	4.16 x 10 ³	9.22 x 10 ⁵	2.64 x 10 ⁴	7.14 ± 0.31	---
GT058	C	76.53816	-68.39758	158	1.15 x 10 ⁵	3.78 x 10 ³	7.45 x 10 ⁵	2.13 x 10 ⁴	6.48 ± 0.28	5.45 x 10 ⁴

^aSample names followed by (R) are those interpreted to have only experienced the most recent period of exposure; these ages w

^bDescribes the sedimentary unit from which the boulder was collected (C = clay-rich diamict, S = sandy diamict, see Fig. 1)

^cRatios and ratio uncertainties for ¹⁰Be/⁹Be and ²⁶Al/²⁷Al are included in the data repository.

^dThe correction for the most recent period of exposure is the average ¹⁰Be apparent exposure age of the three youngest samples whose corrected ratios are consistent with burial; these are the samples for which exposure/burial modelling was condu

Sample Name ^a	Sed. Unit ^b	Single-Nuclide Apparent Exposure Ages ^c		Paired-Nuclide Minimum Limiting Durations and Uncertainties ^d						
		¹⁰ Be Age (ka)	²⁶ Al Age (ka)	Exposure Duration	1 σ Exposure Unc. (ky)	1 σ Exposure Unc. (%)	Burial Duration	1 σ Burial Unc. (ky)	1 σ Burial Unc. (%)	Total History
GT014	C	22.3	21.7	13	1	7	88	92	105	111
GT015	C	29.4	26.9	22	2	7	267	112	42	300
GT016	C	27.3	24.3	21	1	6	378	80	21	410
GT018	C	28.7	28.2	---	---	---	---	---	---	---
GT019	C	22.7	20.1	16	1	5	458	75	16	484
GT021	C	77.5	59.0	96	4	4	627	55	9	734
GT022 ^(R)	C	10.7	10.7	---	---	---	---	---	---	---
GT023 ^(R)	C	10.6	11.6	---	---	---	---	---	---	---
GT027	S	28.0	29.7	---	---	---	---	---	---	---
GT030	S	22.9	23.3	---	---	---	---	---	---	---
GT035	S	23.2	24.2	---	---	---	---	---	---	---
GT036	S	23.7	20.7	18	1	7	491	88	18	520
GT038	S	12.0	12.3	---	---	---	---	---	---	---
GT039	S	11.8	14.8	---	---	---	---	---	---	---
GT040	S	20.4	23.1	---	---	---	---	---	---	---
GT042	S	25.8	26.8	---	---	---	---	---	---	---
GT043	S	26.9	27.7	---	---	---	---	---	---	---
GT044	S	16.5	17.3	---	---	---	---	---	---	---
GT049	S	25.2	26.6	---	---	---	---	---	---	---
GT050	S	18.1	18.4	---	---	---	---	---	---	---
GT051	S	21.3	23.5	---	---	---	---	---	---	---
GT052	S	23.1	24.3	---	---	---	---	---	---	---
GT053	S	19.0	18.8	---	---	---	---	---	---	---
GT054	C	18.5	16.6	11	1	8	493	105	21	515
GT055 ^(R)	C	10.7	11.8	---	---	---	---	---	---	---
GT056	C	22.2	23.1	---	---	---	---	---	---	---
GT057	C	27.2	28.7	---	---	---	---	---	---	---
GT058	C	23.8	22.7	15	1	7	142	91	64	168

^aSample names followed by (R) are those interpreted to have only experienced the most recent period of exposure; these ages were used to correct the remaining samples.

^bDescribes the sedimentary unit from which the boulder was collected (C = clay-rich diamict, S = sandy diamict, see Fig. 1)

^cAges were calculated using the northeastern North American production rates of 3.93 ± 0.19 atoms $\text{g}^{-1} \text{yr}^{-1}$ for ¹⁰Be and 26.5 ± 1.3 atoms $\text{g}^{-1} \text{yr}^{-1}$ for ²⁶Al (Balco et al., 2009) and the Lal (1991)/Stone (2001) scaling scheme in CRONUS. Ages have been scaled for elevation, sample density, sample thickness, latitude, and longitude.